

Microstructural properties of electrochemically synthesized ZnSe thin films

T. Mahalingam · V. Dhanasekaran ·
R. Chandramohan · Jin-Koo Rhee

Received: 12 July 2011 / Accepted: 21 September 2011 / Published online: 8 October 2011
© Springer Science+Business Media, LLC 2011

Abstract In this study, we report the electrosynthesis of zinc selenide (ZnSe) thin films on indium-doped tin oxide-coated glass substrates. The deposited ZnSe thin films have been characterized for structural (X-ray diffraction), surface morphological (scanning electron microscopy), compositional (energy dispersive analysis by X-rays), photoluminescence property, and optical absorption analysis. Formation of cubic structure with preferential orientation along the (111) plane was confirmed from structural analysis. In addition, the influence of the deposition potential on the microstructural properties of ZnSe is plausibly explained. The optical properties of ZnSe thin films are estimated using the transmission spectrum in the range of 400–1200 nm. The optical band gap energy of ZnSe thin films was found to be in the range between 2.52 and 2.61 eV. Photoluminescence spectra were observed at blue shifted band edge peak. The morphological studies depict that the spherical and cuboid shaped grains are distributed evenly over the entire surface of the film. The sizes of the grains are found to be in the range between 150 and 200 nm. The ZnSe thin film stoichiometric composition was observed at optimized deposition condition.

Introduction

Semiconducting nanomaterials exhibit many physical phenomena with some novel optical and transport properties, which are potentially useful for technological point of view especially in light emitting diodes, piezoelectric devices, and photodetectors [1]. Zinc selenide (ZnSe) is an n-type semiconducting material with wide band gap (2.7 eV). It is a suitable material for red, blue, and green light emitting diodes, photovoltaic, laser screens, thin film transistors, photoelectrochemical cells, etc. [2–5]. Now days, ZnSe thin film has been used as n-type window layer for thin film heterojunction solar cells. Though ZnSe has a direct wide band gap (2.7 eV), it is exceptionally interesting material for the applications like optoelectronics, especially for fabrication of the blue light diodes, also it acts as a buffer/window layer in chalcogenide-based thin film solar cells [6, 7].

There are several reports available on the growth of ZnSe thin films by various techniques such as Molecular beam epitaxy [3], chemical vapor deposition (CVD) [6], screen printing [8], vacuum evaporation [9], pulsed laser deposition (PLD) [10], chemical bath deposition (CBD) [11], etc. It has been identified that the deposition from aqueous solution makes the process simple, economical, and easily scalable. Electrodeposition is one of the most widely accepted techniques for the economical and efficient growth of the films from aqueous solution, and numerous reports are available on the deposition of various thin films by this technique. However, it is very surprising to note that the electrodeposition of ZnSe thin films has not been studied in comparison with cadmium chalcogenides. Also it is worth to note that electrodeposition of the ZnSe is difficult because of the wide difference in the reduction potential of Zn and Se ions [12], and only few reports are

T. Mahalingam (✉) · V. Dhanasekaran
Department of Physics, Alagappa University,
Karaikudi 630 003, India
e-mail: maha51@rediffmail.com; tmaha51@yahoo.com

R. Chandramohan
Department of Physics, Sree Sevugan Annamalai College,
Devakottai 630 303, India

J.-K. Rhee
Millimeter-wave INnovation Technology Research Center
(MINT), Dongguk University, Seoul 100-715, Republic of Korea

available on the electrodeposition of ZnSe thin films [13–15]. In this study, ZnSe thin films have been synthesized on indium-doped tin oxide (ITO)-coated conducting glass substrates at various deposition potentials from aqueous electrolytic bath using cathodic electrodeposition technique. The ZnSe films deposited are characterized for structural studies, surface morphological, and optical properties.

Experimental

Electrochemical experiments were carried out using a Potentiostat/Galvanostat (EG&G Princeton Applied Research, USA Model 362A). Electrodeposition was performed in a conventional three electrode cell with ITO substrates as cathode and graphite rod as anode and a saturated calomel electrode as reference electrode. ZnSe thin films were prepared using an electrolyte containing zinc sulfate (ZnSO_4) and SeO_2 . ZnSO_4 and SeO_2 were taken with 0.02 and 0.005 M, respectively. Electrodeposition was performed with deposition potential varying from -0.650 to -0.950 V in steps of 100 mV with respect to SCE. The electrolytic bath temperature and deposition time were maintained at 75°C and 30 min, respectively. Thickness of the deposited films was measured using stylus profilometer (Mitutoyo SJ 301). An X-ray diffractometer (X'PERT PRO PANalytical, Netherlands) with $\text{CuK}\alpha$ radiation ($\lambda = 0.1540$ nm) was used to identify the crystal structure of the films. Surface morphological studies were carried out using energy dispersive analysis attached with scanning electron microscopy (SEM-Philips Model XL 30, USA). Photoluminescence (PL) spectroscopic studies were carried out using Variant Cary Eclipse Fluorescence Spectrophotometer.

Results and discussion

Thickness measurement

Figure 1 represents the variation of film thickness with deposition time for ZnSe thin films prepared at various deposition potentials. Thickness of all the films increase linearly with the deposition time initially up to 20 min for all the deposition potential and after this deposition time it shows non-linearity behavior. Moreover, the film thickness tends to attain saturation after 40 min of deposition time. Further, we observe fewer adherents, uncontrolled and non-reproducible growth rate for the deposition potential increases above -650 mV versus SCE. The increase in film thickness is described by the following two mechanisms: the deposition of ZnSe leading to the film growth

and the reaction of formation of ZnSe with acid in time being prolonged; so that the thickness of the film increases, at the same time the resistance of the film also increases. Eventually, the density of electrons decreases relatively and the ZnSe thin films were eroded by acid in the solution. Therefore, after a particular time of deposition, the dissolution process predominates over the deposition thereby results to indicate decrease in film thickness. In micro-electronic applications, the film thickness is to be scaled down to the device size. So, it is valuable to examine the effect of film thickness on the physical properties of ZnSe thin films which is valuable to examine how ZnSe micro-structure evolves with thickness and affects physical properties. It is observed that the film thickness gradually increases with deposition potential when other parameters such as bath temperature and deposition time are kept constant.

Structural studies

X-ray diffraction patterns are recorded for ZnSe thin films synthesized at different deposition potentials ranging from -650 to -950 mV versus SCE in steps of 100 mV by maintaining the deposition time and bath temperature at 30 min and 75°C , respectively, shown in Fig. 2. X-ray diffraction studies revealed that the deposited films were polycrystalline in nature with cubic structure. The X-ray diffraction patterns show diffraction peaks at angles 27.25° , 31.43° , 45.10° , 53.65° , 65.71° , and 72.11° corresponding to crystallographic orientations (111), (200), (220), (311), (400), and (331), respectively. The observed peaks “*d*” spacing values are in good agreement with standard JCPDS card no. 88-2345 for ZnSe. The strongest diffraction peak appears at 27.25° that correspond to (111)

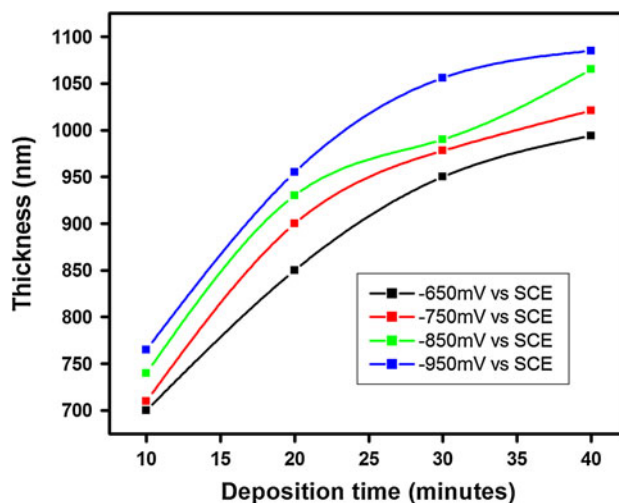


Fig. 1 Variation of film thickness with deposition time for ZnSe thin films obtained at various deposition potentials

plane. The line width of (111) peak, which is 0.21° for -650 mV versus SCE prepared film, increases largely with increasing deposition potential and reaches 0.18° , implying that the crystallite size of the ZnSe films increases with the deposition potential. For further decrease in deposition potential, the films show improved crystalline structure and the intensity of (111) plane increases to maximum up to potential -950 mV versus SCE. Above this precursor deposition potential, the intensity (311) peak is reduced and the (331) peak is slightly increased. However, both the peaks seem to have intensities less than the (111) peak. The average crystallite size is found to be 39 nm for the maximum deposition potential and 44 nm for the more negative potential. The structural studies revealed that the cubic structure of ZnSe is conserved. However, one ZnSe satellite peak corresponding to (200) emerged in addition to the conventional ZnSe peaks (111) and (311) during the increase of deposition potential. These satellite peaks are exposed to increase crystallinity of ZnSe thin films with increasing deposition potential.

The predominant peak orientation (111) crystallographical plane is observed in all the XRD patterns. From the (hkl) planes, the lattice constants were evaluated using the relation,

$$d = \left[\frac{a}{\sqrt{(h^2 + k^2 + l^2)}} \right] \quad (1)$$

where d is the inter-planar spacing of the atomic plane. From the X-ray diffraction line broadening it is observed that the inter-atomic distance between the two atoms decrease with increase of deposition potential and the magnitudes are shown in Table 1. The calculated d -spacing values have been used to determine the lattice constant and values are also tabulated in Table 1. The full width at half-maximum (FWHM) is important to calculate the some microstructural parameters of the films and are included in Table 1. The standard values of diffraction angles are compared with observed diffraction angle and from the change of diffraction angle several structural parameters are evaluated and presented in the Table 1.

The texture coefficient was calculated using an expression

$$P(h_i k_i l_i) = \frac{I(h_i k_i l_i)}{I_0(h_i k_i l_i)} \left[\frac{1}{n} \sum \frac{I(h_i k_i l_i)}{I_0(h_i k_i l_i)} \right]^{-1} \quad (2)$$

where I_0 represents the standard intensity, I is the observed intensity of $(h_i k_i l_i)$ plane, and n is the reflection number. The crystallite shape of the ZnSe thin film is strongly related to the texture of ZnSe film. The predominant plane orientation of the film has high texture coefficient value. The various crystallographic planes such as (111), (200), (220), (311), (400), and (331) texture coefficient values are

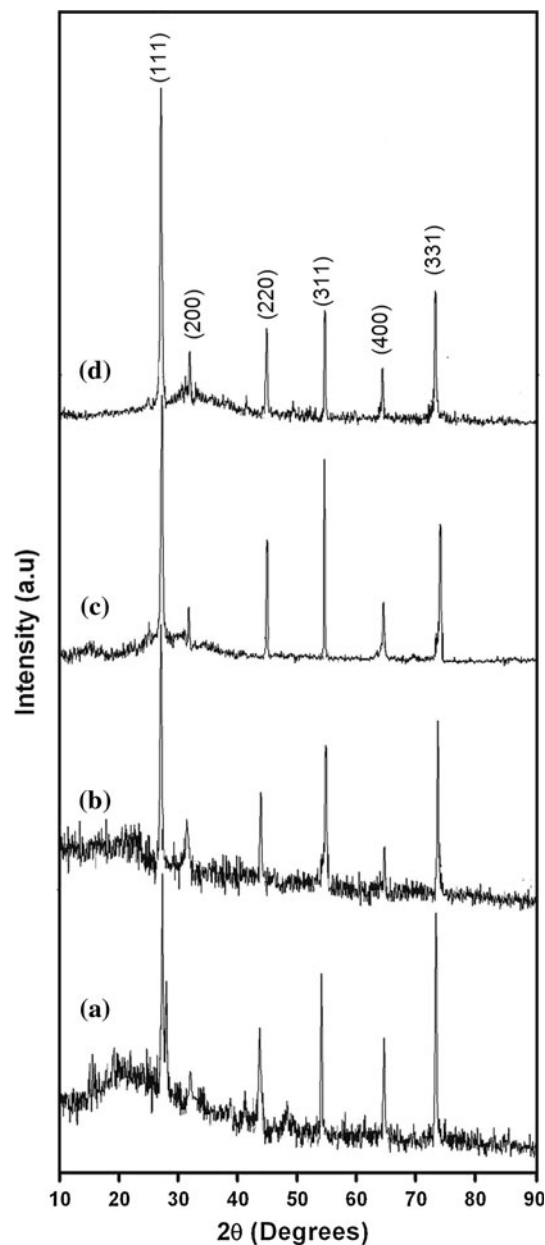


Fig. 2 X-ray diffractogram of ZnSe thin films at various deposition potentials (a) -650 mV, (b) -750 mV, (c) -850 mV, and (d) -950 mV versus SCE

calculated. The maximum texture coefficient value is found to be 2.41 at deposition potential -950 mV versus SCE. Also, the texture coefficient along (111) plane is found to be decreasing with increase in deposition potential as shown in Table 1. So that texture coefficient is higher than 1 indicates preferential orientation and also indicates the abundance of grains in a given (h_i, k_i, l_i) direction.

The microstructural parameters are calculated using an X-ray diffraction patterns. The crystallite size and micro-strain for the electrodeposited ZnSe films were obtained from FWHM which can be expressed as linear combination

Table 1 Basic XRD parameters and texture coefficient of ZnSe thin films

S. no.	Deposition potential (mV vs. SCE)	d -spacing (Å)	Lattice constant (Å)	Full width at half maximum (FWHM) in radians	$\Delta(2\theta)$ in radians	Texture coefficient (T_C)
1	−650	3.282	5.684	0.00366	0.00558	2.28
2	−750	3.283	5.686	0.00352	0.00314	2.34
3	−850	3.284	5.687	0.00336	0.00296	2.38
4	−950	3.286	5.691	0.00324	0.00157	2.41

of contributes from the particle size, D and strain ε given below. The crystallite size D of the films was calculated from the Debye Scherer’s formula from the FWHM intensity expressed in radians

$$D = \frac{0.9\lambda}{\beta \cos \theta} \tag{3}$$

where D is crystallite size and β is the FWHM. The origin of the micro strain is related to the lattice misfit, which in turn depends upon the deposition conditions. The crystallite size can be controlled simply by varying the applied deposition potential. The crystallite size is found to be in the range between 44 and 39 nm for deposition potentials ranging from −950 to −650 mV versus SCE and tabulated in Table 2. The crystallite size is found to decrease gradually with increase deposition potential from −950 to −650 mV versus SCE. We attribute that crystallite size decreases with increase of deposition rate. The micro strain ε is calculated using the relation [16],

$$\frac{\beta \cos \theta}{\lambda} = \frac{1}{D} + \frac{\varepsilon \sin \theta}{\lambda} \tag{4}$$

where λ is wavelength and θ is Bragg’s angle. In general, the crystallite size is indirectly proportional to microstrain. Table 2 represents micro strain with various deposition potentials. Initially, the micro strain increases slowly with deposition potential and minimum microstrain 0.002 is obtained at −950 mV versus SCE. This suggests that crystallinity and preferential orientation increases with decreasing deposition potential.

The dislocation density δ , defined as the length of dislocation lines per unit volume of the crystal, is evaluated from the crystallite size D and microstrain (ε) by the relation,

$$\delta = \frac{15\varepsilon}{aD} \tag{5}$$

where ‘ a ’ is lattice constant. The number of crystallites per unit area (N) of the films was determined with the using formula,

$$N = \frac{t}{D^3} \tag{6}$$

where t is thickness of the film, N number of crystallites per unit area, and D crystallite size. Table 2 represents the dislocation density (δ) and the number of crystallites per unit area (N) of electrodeposited ZnSe thin films with different deposition potentials. Dislocation density and number of crystallites per unit area are increasing with increase in deposition potential. The maximum value of dislocation density and number of crystallites per unit area are found to be 6.4×10^{14} lines/m² and 1.4×10^{16} , respectively, for the film deposited at −650 mV versus SCE. This is found to rapidly increase with increase in deposition potential from −950 to −650 mV versus SCE which may be attributed to the reduction in crystallite size with increase in deposition potential shown in Table 2.

The stacking fault probability was calculated by measuring the peak shift and tangent values of diffracting angle,

$$\alpha = \left[\frac{2\pi^2}{45\sqrt{3}} \right] \left[\frac{\Delta(2\theta)}{\tan \theta_{111}} \right]. \tag{7}$$

The stacking fault probability of the ZnSe thin films is found to be in the range between 0.0016 and 0.0057. The calculated values are tabulated in Table 2. The crystals defect parameters like microstrain, number of crystallites per unit area, stacking fault probability, and dislocation density show an increasing trend with increase in

Table 2 Micro structural properties of electrodeposited ZnSe thin films with various deposition potentials

S. no.	Deposition potential (mV vs. SCE)	Crystallite size (nm)	Micro strain (ε) $\times 10^{-3}$ lines ^{−2} m ^{−4}	Dislocation density lines/m ² (10^{14})	Number of crystallites per unit area (10^{16}) m ^{−2}	Stacking fault probability (α) (10^{-3})
1	−650	39.0	6.2	6.6	1.3	5.76
2	−750	40.5	4.5	6.1	1.2	3.26
3	−850	42.5	3.7	5.5	1.0	3.12
4	−950	44.0	2.0	5.2	0.93	1.63

deposition potential. This type of change in strain may be due to the recrystallization process in the polycrystalline films. In the higher deposition potential, the microstructural properties are maximum which reveals the reduction in the concentration of lattice imperfections leading to preferred orientations.

Figure 3 illustrates the plot of $\Delta(2\theta) \cos\theta_0$ versus $\sin\theta_0$, and the values of ε and D can be calculated from the slope and the ordinate intersection, respectively. Equation 8 was first proposed by Williamson and Hall [17] and is customarily referred to as the “Williamson–Hall method”.

$$\Delta(2\theta) \cos \theta_0 = \frac{\lambda}{D} + 4\varepsilon \sin \theta_0. \quad (8)$$

From this above Eq. 8, we have to calculate crystallite size and microstrain using intersection of y axis and plot the slope, respectively.

Figure 4 shows a comparison between the estimated crystallite size of the electrodeposited ZnSe thin films with various deposition potentials obtained by calculation and graphical method. Graphical crystallite sizes have been calculated using Eq. 8. The graphical crystallite size is found to be slightly high value compared with calculated value deposited at -950 mV versus SCE. The significant observation from these estimations is that at the optimized deposition potential the two values coincide establishing that this technique can be used for optimization of deposition potential. Similarly, the microstrain estimation can also be used for optimization. Figure 5 shows the estimated microstrain using calculation and from graph for different deposition potentials. The graphical value of microstrain linearly decreases with deposition potential and the lower values were found for graphical method compared to calculated values. At the optimized deposition potential, these values are coinciding and hence -850 mV versus SCE was

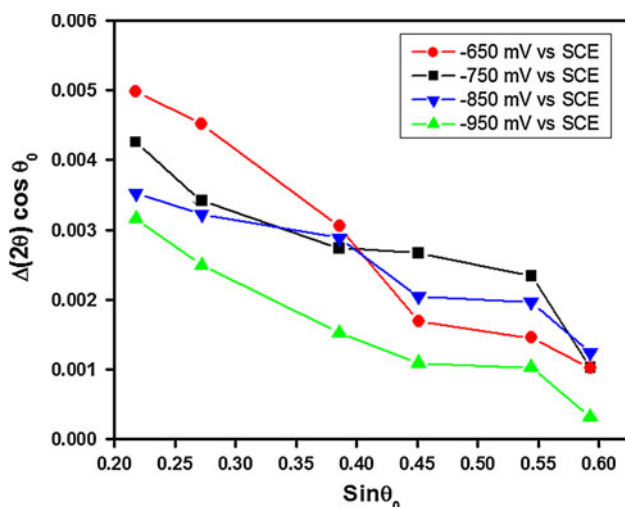


Fig. 3 Plot of Williamson–Hall equation $\sin\theta$ versus $\Delta(2\theta) \cos\theta$

chosen for further preparations. The SEM studies also revealed the uniform-sized grains for the samples coated at -850 mV versus SCE and will be discussed separately.

Optical studies

Optical transmission spectra were recorded at room temperature in air to obtain information on the optical properties of ZnSe thin films. Figure 6 shows the transmittance spectrum obtained for ZnSe films prepared by electrodeposition at different deposition potentials. The transmittance spectrum shows the surface plasmons resonance indicating the crystallite sizes in the nanometer range. The transmittance increases as the deposition potential decreases and it tends to increase in the IR region for all the films it may be due to the film thickness. The increase in the transmittance is due to an increase in the band gap with carrier concentration. It is observed that transmittance increases with the wavelength from 40 to 80%. The maximum range of deposition potential film displays the spectra with lesser transmittance. The nature of transition is determined using the following equation [16],

$$\alpha hv = A(hv - E_g)^n \quad (9)$$

where α is absorption coefficient in cm^{-1} , $h\nu$ is photon energy, E_g is an energy gap, A is energy dependent constant, and n is an integer depending on the nature of electronic transitions. For the direct allowed transitions, n has a value of $1/2$ while for the indirect allowed transitions, $n = 2$. The band gap variation of ZnSe thin films with deposition potential is as shown in Table 3. Figure 7 shows Tauc’s plot of ZnSe thin film deposited at -850 mV versus SCE. From this graph, band gap energy estimated to be 2.52 eV and inset Fig. 7 shows band gap energy

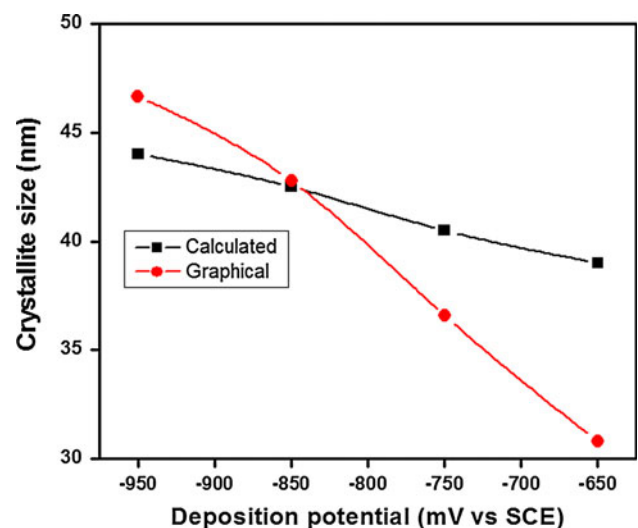


Fig. 4 Crystallite size values comparison using Debye–Scherrer and graphical method

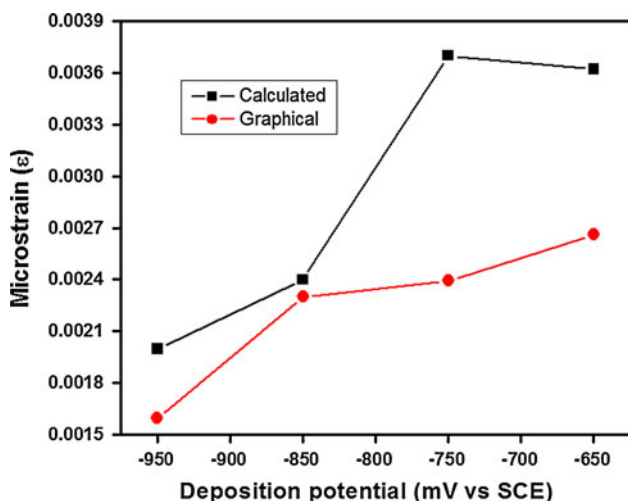


Fig. 5 Micro strain values comparison using Eq. 4 and graphical method

confirmation of differential transmittance method. The energy band gap estimation using the two methods agreed well. One can use the differential transmittance method to verify if the slope estimated in the Taucs plot is correct and extend the same for their estimation. The energy band gap of films deposited at different deposition potentials was found to be in the range of 2.52–2.61 eV using the conventional Tauc’s plot method as shown in Table 3. This increase in the energy band gap with increase of film thickness may be due to quantum confinement.

PL spectra were recorded at room temperature using an emission wavelength of 421 nm. The spectra show peaks at 378 and 383 nm (Fig. 8), respectively, and the PL intensity was found to increase with decrease deposition potential. These peaks are assigned to the near band emission. Self

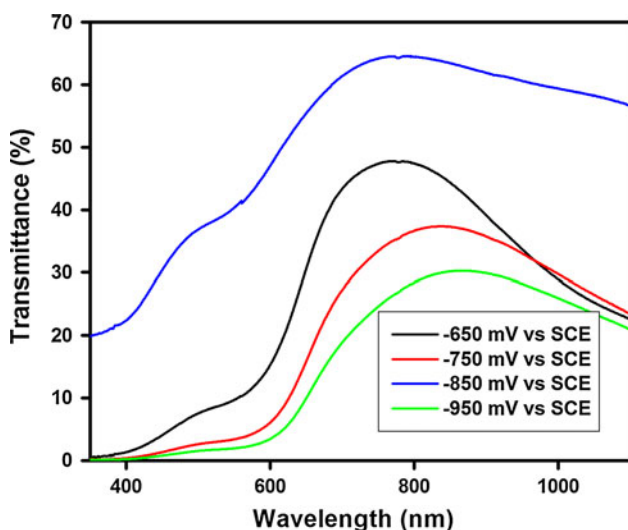


Fig. 6 Transmittance spectra of electrodeposited ZnSe thin films for various deposition potentials

activated centers arising from complexes of zinc vacancies and shallow donors (selenium interstitials) would occur around 379 eV [18]. The PL emission from the undoped ZnSe has been attributed to the presence of native defects like zinc and selenium vacancies or interstitials, which are likely to be introduced during the growth process [19, 20]. Note that all the samples exhibited PL peaks at 383 nm, which is slightly blue shifted with respect to the value of absorption onset at 420 nm for ZnSe. The closeness of PL peak position with the absorption edge implied that the luminescence is related to the band edge recombination in the ZnSe thin films. Interestingly, the emission spectra of ZnSe sample exhibited considerable enhancement in the luminescence by a factor of ZnSe film. It is known that the nano level crystallite size generally poses a high density of surface state. These surface states may act as traps for the photo excited carriers and may suppress excitonic luminescence [21] considerably. This result may be attributed to effective distribution of surface states into ZnSe matrix, thereby enhancing the luminescence yield. Therefore, the ZnSe system may be an attractive choice for application as displays and solar cells.

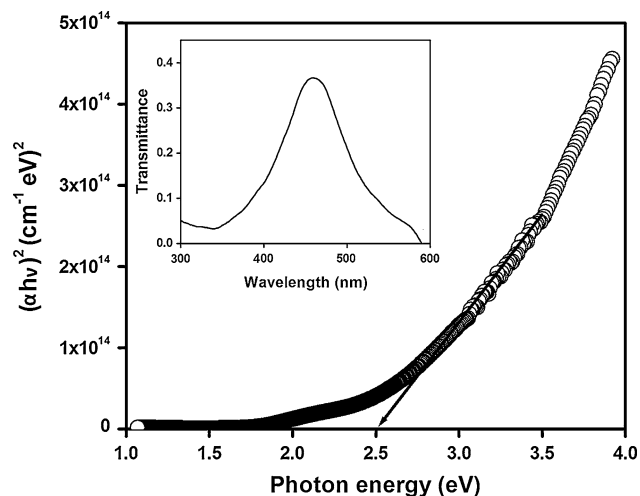
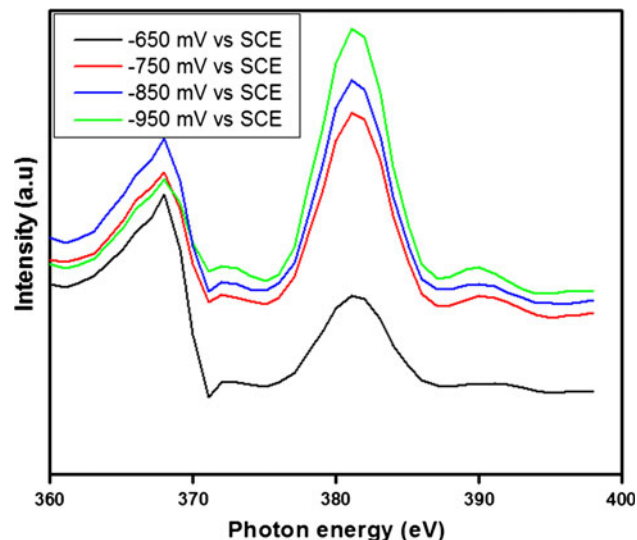
Morphological and compositional studies

The surface morphology of ZnSe thin films was analyzed using a scanning electron microscope. The scanning electron microscope image of ZnSe thin films prepared at different deposition potentials (–650 and –850 mV versus SCE) is shown in Fig. 9a, b. It is observed from Fig. 9a that the film surface is observed to be flat and no definite grain structure is observed for films prepared at deposition potential –650 mV versus SCE. It is also observed that some holes are seen at few places in the SEM picture. For the high deposition potential (–650 mV versus SCE), the deposited films look very thin having a lot of irregularities and exhibiting amorphous nature. Figure 9b represents that the film surface is found to be uniform and covered with small cuboid-shaped grains. The grains are distributed evenly over the entire surface of the film. The sizes of the grains are found to be in the range between 150 and 200 nm. The average size of the grains is found to be 175 nm. This result implies that there is an increase in nucleation over-growth and the deposits are more compact with uniform grain structure. A decrease in the size of the crystallites with deposition potential was also evident from the SEM picture.

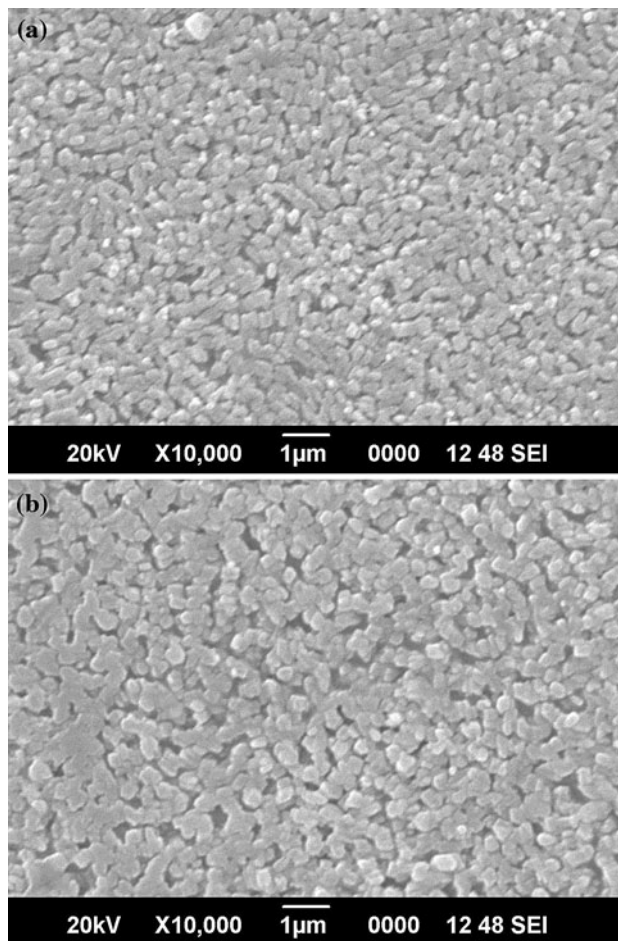
Figure 10 shows the EDX spectrum of ZnSe thin films obtained at deposition potential of –850 mV versus SCE. The presence of emission lines in the investigated energy range indicates the formation of ZnSe thin films. The atomic molar ratio (Zn:Se) of ZnSe (47.94:52.06) thin films obtained at deposition potential –850 mV versus SCE is

Table 3 Composition and band gap of electrodeposited ZnSe thin films

S. no.	Deposition potential (mV vs. SCE)	Composition of elements (%)		Band gap in eV (E_g)
		Zinc	Selenium	
1	–650	35.73	64.27	2.61
2	–750	41.90	58.10	2.58
3	–850	47.94	52.06	2.52
4	–950	55.05	44.95	2.54

**Fig. 7** Tauc's plot of ZnSe thin film deposited at –850 mV versus SCE (*Inset* figure shows differential transmittance spectra for confirmation of conventional method band gap value)**Fig. 8** Photoluminescence spectra of ZnSe thin films

found to be near stoichiometric formation of good quality ZnSe thin films. This result is also consistent with X-ray diffraction analysis of the sample with cubic phase

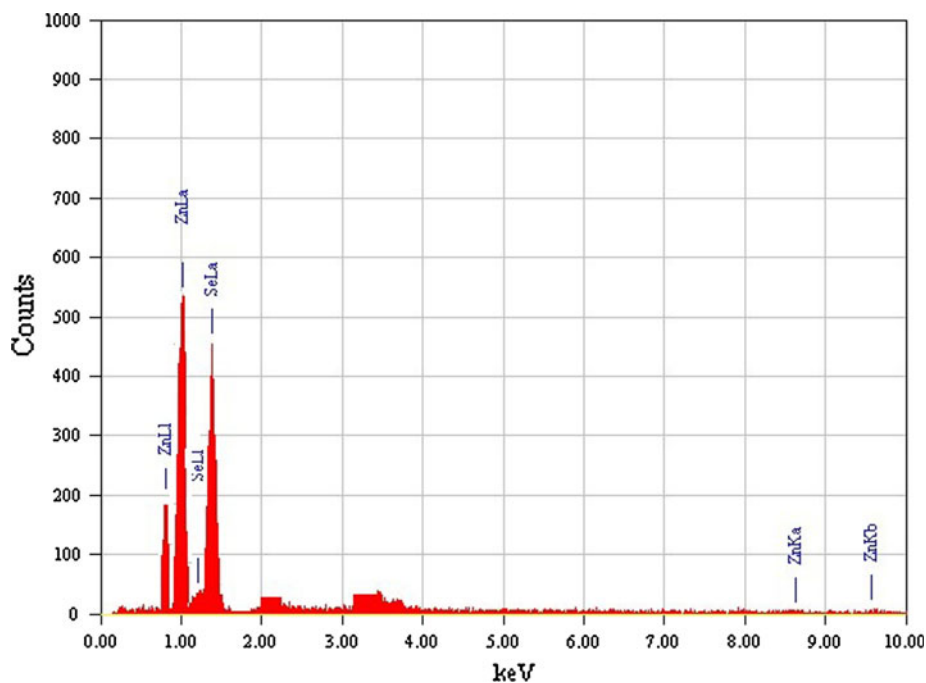
**Fig. 9** SEM pictures of ZnSe thin films obtained at different deposition potentials: **a** –650 mV and **b** –850 mV versus SCE

corresponding to ZnSe. The atomic percentage of Zn and Se obtained at deposition potential –850 mV versus SCE is found to be in close agreement with the value reported earlier for brush-plated ZnSe thin films [18]. Table 3 shows composition of electrodeposited ZnSe thin films at various deposition potentials. Further exploration of electrodeposition technique to tailor the stoichiometry of ZnSe and estimating their properties is under progress.

Conclusions

Thin films of ZnSe were electrodeposited on indium-doped tin oxide-coated conducting glass substrate from an aqueous electrolytic bath using potentiostatic electrodeposition technique. The presence of the XRD pattern represents that the deposited films were found that polycrystalline in nature with cubic structure with preferential orientation along (111) plane. Also the microstructural parameters such as texture coefficient, crystallite size, strain, dislocation density, stacking fault probability, and number of crystallites

Fig. 10 Typical EDX spectrum of ZnSe thin film deposited at -850 mV versus SCE



per unit area are estimated and they are found to sensitive with deposition potentials. The SEM results represent that the films at -850 mV versus SCE deposition potential have surface with spherical-shaped grains. SEM micrographs show that the present films are uniform, homogeneous, and well covered on the substrate. From the surface morphological studies, we could conclude that the deposition potential plays a beneficial role while formation of thin layers of ZnSe on it. The stoichiometric composition of ZnSe thin film is observed at pH 2.5. The sizes of the grains are found to be in the range between 150 and 200 nm. Optical characterization of the film shows the characteristic transition of semiconductive ZnSe thin films band gap energy 2.52 eV at -850 mV versus SCE. Therefore, the ZnSe system may be an attractive choice for application as displays and solar cells.

References

1. Son D, Jung DR, Kim J, Moon T, Kim C, Park B (2007) *Appl Phys Lett* 90:101910
2. Akira O, Noriyoshi S, Zembutsu S (1988) *J Appl Phys* 64:654
3. Ennaoui A, Siebntritt S, Lux-Steiner MCh, Riedl W, Karg F (2001) *Sol Energy Mater Sol Cells* 67:31
4. Alfano RR, Wang OZ, Jumbo J, Bhargava B (1987) *J Phys Rev A* 35:459
5. Chaparro AM, Gutierrez MT, Herrero J, Klaer J (2001) *Mater Res Soc Symp Proc* 668:H2.9.1
6. Rumberg A, Sommerhalter C, Toplak M, Jager-Waldau A, Lux-Steiner MC (2000) *Thin Solid Films* 361–362:172
7. Chu TL, Chu SS, Chen G, Britt J, Ferekides C, Wu CQ (1992) *J Appl Phys* 71:8
8. Kumar V, Khan KLA, Singh G, Sharma TP, Hussain M (2007) *Appl Surf Sci* 253:3543
9. Venkatachalam S, Mangalaraj D, Narayandass SK (2007) *Physica B* 393:47
10. Ryu YR, Zhu S, Han SW, White HW, Miceli PF, Chandrasekhar HR (1998) *Appl Surf Sci* 127:496
11. Kale RB, Lokhande CD, Mane RS, Han S-H (2006) *Appl Surf Sci* 252:5768
12. Chandramohan R, Sanjeeviraja C, Mahalingam T (1997) *Phys Status Solidi b* 163:R11
13. Bouroushian M, Kosanovic T, Spyrellis N (2005) *J Cryst Growth* 277:335
14. Kosanovic T, Bouroushian M, Spyrellis N (2005) *Mater Chem Phys* 90:148
15. Riverous G, Gomez H, Henriquez R, Schreiber R, Marotti RE, Dalchiele EA (2001) *Sol Energy Mater Sol Cells* 70:255
16. Mahalingam T, Dhanasekaran V, Ravi G, Lee S, Chu JP, Lim H (2010) *J Optoelectron Adv Mater* 12:1327
17. Morris DG, Morris MA, LeBoeuf M (1992) *Mater Sci Eng A* 156:11
18. Murali KR, Austine A, Trivedi DC (2005) *Mater Lett* 59:2621
19. Yodo T, Ueda R, Morio K, Yamasita R, Tanaka S (1990) *J Appl Phys* 68:3212
20. Sokurai F, Suto K, Sanda S, Nishizawa J (2002) *J Electrochem Soc* 149:G100
21. Manar A, Chergui A, Guennani D, Ohlmann D, Cloitre T, Aulombard RL (1997) *Mater Sci Eng B* 43:121